Pinhole SPECT: An Approach to In Vivo High Resolution SPECT Imaging in Small Laboratory Animals

D.A. Weber, M. Ivanovic, D. Franceschi, S-E. Strand, K. Erlandsson, M. Franceschi, H.L. Atkins, J. A. Coderre, H. Susskind, T. Button and K. Ljunggren

Medical Department, Brookhaven National Laboratory, Upton, New York; Radiation Physics Department, University of Lund, Lund, Sweden; University Hospital Sestre Milosrdnice, Zagreb, Croatia; and Department of Radiology, Health Science Center, State University of New York, Stony Brook, New York

The performance of pinhole SPECT and the application of this technology to investigate the localization properties of radiopharmaceuticals in vivo in small laboratory animals are presented. **Methods:** System sensitivity and spatial resolution measurements of a rotating scintillation camera system are made for a low-energy pinhole collimator equipped with 1.0-, 2.0- and 3.3-mm aperture pinhole inserts. The spatial detail offered by pinhole SPECT for in vivo imaging was investigated in studies of the brain and heart in Fisher 344 rats by administering ^{201}TlCl, ^{99m}Tc-HMPAO, ^{99m}Tc-DTPA and ^{99m}Tc-MIBI. Image acquisition is performed using a rotating scintillation camera equipped with a pinhole collimator; projection data are acquired in conventional step-and-shoot mode as the camera is rotated 360° around the subject. Pinhole SPECT images are reconstructed using a modified cone-beam algorithm developed from a two-dimensional fanbeam filtered backprojection algorithm. **Results:** The reconstructed transaxial resolution of 2.8 mm FWHM and system sensitivity of 0.086 c/s/kBq with the 2.0-mm pinhole collimator aperture provide excellent spatial detail and adequate sensitivity for imaging the regional uptake of the radiopharmaceuticals in tumor, organs and other tissues in small laboratory animals. **Conclusion:** The resolution properties of pinhole SPECT are superior to those which have been achieved thus far with conventional SPECT or PET imaging technologies. Pinhole SPECT provides an important approach for investigating localization properties of radiopharmaceuticals in vivo.

Key Words: pinhole SPECT; tumor imaging; technetium-99m-DTPA; technetium-99m-MIBI; technetium-99m-HMPAO; thallium-201-chloride

J Nucl Med 1994; 35:342–348

Improvements in spatial resolution for in vivo imaging are continuously being sought in nuclear medicine to increase the spatial detail that can be obtained in internal emitter imaging studies. The expanding number and improved availability of labeled antibodies, receptor agents and other new radiopharmaceuticals for imaging and therapy (1–3) place new demands on the need for high spatial resolution techniques to investigate the regional localization properties of these radiopharmaceuticals in preclinical and clinical studies.

Planar imaging of the activity distribution of radiopharmaceuticals in laboratory animals has been conventionally performed using scintillation camera techniques with high-resolution parallel-hole collimators or pinhole collimators. Although reasonably good spatial resolution can be achieved with these techniques, only two-dimensional images of the three-dimensional activity distribution are obtained, and spatial detail and contrast are limited except for superficially located target tissues due to crosstalk from activity in over- or underlying tissues. Conventional SPECT imaging with parallel-hole, fanbeam, or cone-beam collimators can provide tomograms of the activity distribution in three dimensions. However, the spatial resolution that can be achieved with these collimators has not been adequate to provide the fine detail needed to characterize regional localization properties of radiopharmaceuticals in vivo, in many tissues and organs of small laboratory animals. Despite offering the best combination of spatial resolution and sensitivity for imaging small objects positioned close to the collimator, the use of pinhole collimation for SPECT has received little attention.

Narrow-aperture pinhole collimators can yield significantly better spatial resolution for SPECT provided short imaging distances are used to image small objects and appropriate image reconstruction software is employed. The divergent beam-imaging geometry of the pinhole collimator requires projection data to be processed with an appropriate divergent beam reconstruction algorithm to obtain cross-sectional tomographic slices (4–8). Pinhole SPECT image reconstruction was reported earlier for studies in rabbits (8), and recently several investigators have reported studies designed to develop a practical solution to the need for improved spatial resolution imaging in laboratory animals (4,9,10). Here, we tested the sensitivity and

spatial resolution of smaller pinhole apertures than those conventionally supplied, in order to select a collimator aperture that would be optimum for imaging tracer localization properties in rats and mice. Images were reconstructed using a modified cone-beam filtered backprojection algorithm (4). We identify an approach to SPECT imaging that provides improved spatial resolution for demonstrating localization properties of radiopharmaceuticals in small laboratory animals. The experimentally determined performance properties and examples of high-resolution pinhole SPECT images of the rat's brain and myocardium in vivo are presented. Correlation with other assay techniques are made.

MATERIALS AND METHODS

Pinhole imaging was performed using a rotating scintillation camera equipped with 1.0-, 2.0- and 3.3-mm aperture pinhole inserts in a low-energy pinhole collimator. Pinhole collimator inserts with 1.0- and 2.0-mm diameter apertures fabricated out of lead and a 3.3-mm diameter tungsten insert, supplied with the imaging system, were tested in this study. Performance properties of all three pinhole apertures were measured using a zoom of 2 and an acquisition matrix of 256 × 256 pixels for the 30-cm diameter pinhole field of view (FOV). All pinhole SPECT and planar imaging studies were acquired using a 2.0-mm aperture pinhole collimator and a zoom of 2. SPECT studies were acquired in a 64 × 64-pixel matrix; planar images were acquired in a 128 × 128-pixel matrix. Studies were performed using a 20% energy window, centered on the 140.5-keV gamma photopeak of ^{99m}Tc and the 68.9–82.6 keV x-ray photopeaks of ^{201}Tl. SPECT projections were collected at 4° increments over 360° in the step-and-shoot mode using a 4.5-cm radius of rotation.

Phantom Studies

System sensitivity and spatial resolution measurements with the pinhole collimator were obtained for the three pinhole apertures. Collimator sensitivity was measured at 10-mm increments along the central axis over the range of 20 mm to 150 mm from the pinhole collimator aperture. A 2.2-cm diameter × 2.5-mm thick disk source containing 85 MBq of ^{99m}Tc was counted. Spatial resolution was measured using two capillary tube line sources with active dimensions of 80-mm length × 1-mm diameter, containing ^{99m}Tc (48 MBq/ml). Resolution as a function of distance from a pinhole aperture was determined as the full width at half maximum (FWHM) of the count profiles of the line source at different distances to the collimator.

The spatial resolution of the reconstructed SPECT images for the 2.0-mm pinhole aperture was determined from the count profiles obtained from the transaxial images of a five-line source phantom imaged with a radius of rotation of 4.5 cm (Fig. 1). The phantom consisted of a 3.0-cm diameter × 4.5-cm long Plexiglass rod with five 0.58-mm diameter parallel holes drilled through the length of the phantom to serve as line sources. One hole was positioned in the center of the long axis of the Plexiglass cylinder and the remaining four holes were placed 1.0 cm apart in a square pattern centered around the central axis hole.

The decrease in geometric efficiency (11) and uniformity variations in the pinhole collimator response in the radial direction from the center to the edge of the FOV were measured using a ^{57}Co flood source image. A correction matrix, calculated as a normalization matrix from the inverse of the flood source image, was used to correct projections for variations in geometric effi-
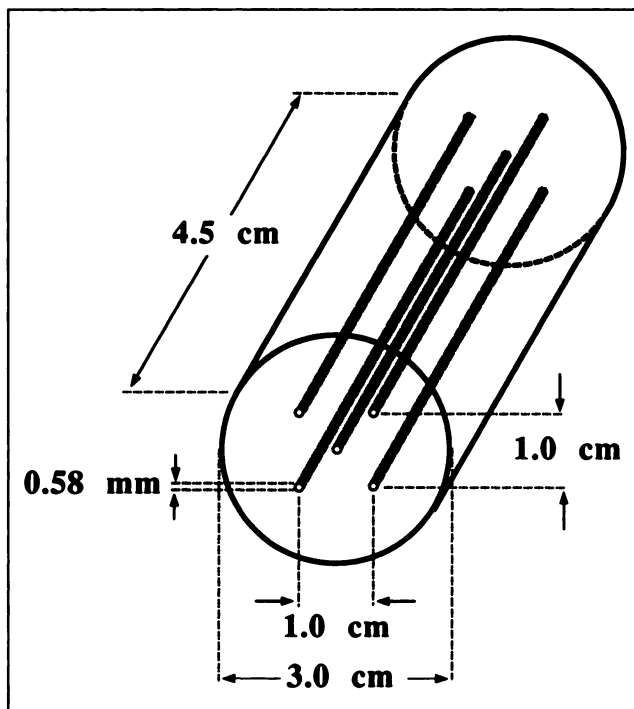

FIGURE 1. Diagram of a five-line source phantom used to assay spatial resolution of pinhole SPECT system.

ciency and field uniformity prior to reconstruction. Projection data were corrected for isotope decay and center-of-rotation shift and a two-dimensional smoothing filter was applied before reconstruction. Image reconstruction was performed using a filtered backprojection algorithm based on a cone-beam algorithm (4,6), which is a generalization of the two-dimensional fanbeam algorithm. The algorithm treats the planes outside the central axial plane as tilted fanbeams. This is an approximation, which results in some degradation of the axial resolution with distance from the central plane (7). In the backprojection process, the magnification for all planes is adjusted to the magnification of the central plane. A pinhole SPECT study with a 2.5-cm diameter sphere filled with 74 MBq of ^{99m}Tc was used to confirm the corrections made in geometric and intrinsic sensitivity.

Animal Imaging Studies

The level of spatial detail offered by pinhole SPECT for in vivo imaging was investigated for studies of the brain and heart in Fisher 344 rats. Imaging studies included an examination of the localization properties of ^{201}TlCl, ^{99m}Tc-HMPAO, ^{99m}Tc-DTPA, and ^{99m}Tc-MIBI in the brains of control rats and in the brains of rats with transplanted primary brain tumors and ^{99m}Tc-MIBI in a control rat's heart. Rats were anesthetized for tumor cell implantation and imaging studies with an intraperitoneal injection of ketamine (120 mg/kg) and xylazine (20 mg/kg). Brain tumor was initiated by inoculation of the GS-9L gliosarcoma cells into the left frontal lobe of the brain in rats weighing 200–220 g (12). Tumor-bearing animals were imaged between 18 and 28 days after tumor cell inoculation when the tumors varied from approximately 6 mm to 12 mm in their largest dimension.

Pinhole SPECT was performed 30 min after the intravenous administration of 37 MBq of ^{201}TlCl, 185 MBq of ^{99m}Tc-DTPA, 185 MBq of ^{99m}Tc-HMPAO and 185 MBq of ^{99m}Tc-MIBI in the tail vein of the rat. The animals were positioned for imaging in a
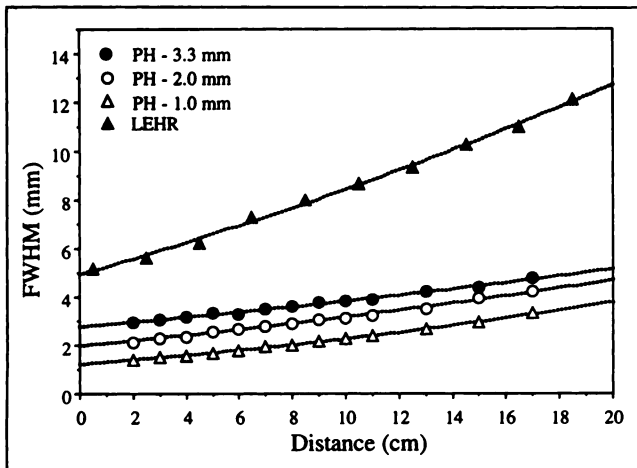
FIGURE 2. Spatial resolution plotted as a function of distance between collimator and ^{99m}Tc line source shows the 1.0-, 2.0-, and 3.3-mm diameter pinhole collimator apertures to have significantly better resolution than LEHR collimator.
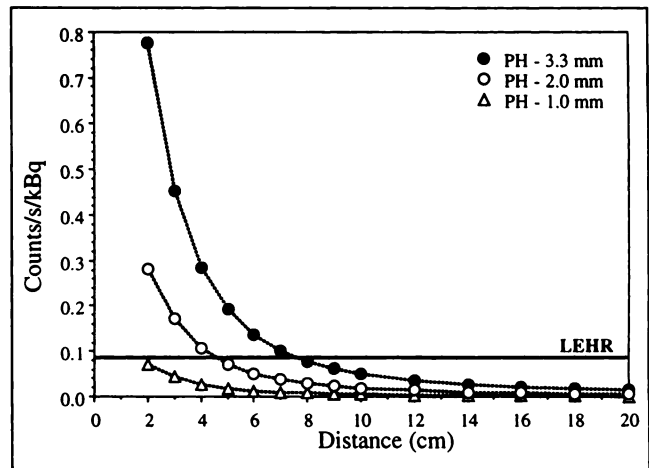

FIGURE 3. Pinhole collimator sensitivity plotted as a function of distance between the collimator and a 2.2-cm diameter disk source of ^{99m}Tc compared with sensitivity of the LEHR collimator.

6.5-cm diameter, cylindrical, cardboard holder, which was attached as an extension to the SPECT imaging platform. The holder accommodated a radius of rotation for SPECT acquisition of ≥3.5 cm. An acquisition time of 30 sec/projection was used. Transaxial, sagittal and coronal slices were reconstructed with a spatial sampling of 0.6 mm; 2-pixel (1.2 mm) thick slices, were used to evaluate distribution properties of the different radiopharmaceuticals. Planar camera images of the brain were recorded in the left lateral view for 20 min immediately before the SPECT study and in the posterior view for 10 min after the SPECT study for comparison. Region of interest (ROI) techniques were used to evaluate differences in radiopharmaceutical uptake in tumor and control normal regions of the brain.

Correlative Studies

MRI imaging of the rat's brain was used to identify tumor and structures within the brain, and to correlate with radiopharmaceutical localization properties on SPECT and planar images. After the imaging procedures were completed, tumor-bearing animals were killed by an overdose of anesthesia and the brain was removed for counting and/or autoradiography. The tumor and brain were separated and measurements of activity were made in a NaI(Tl) well-cup scintillation detector. Conventional film autoradiography and beta-camera autoradiography, using a plastic scintillator and a microchannel plate detector (13), were made on 50-μ thick sections of the brain and tumor in the animal injected with ^{99m}Tc-HMPAO.

The investigational studies in animals were approved by the Institutional Animal Care and Use Committee at Brookhaven National Laboratory.

RESULTS

The spatial resolution of the three different pinhole collimator inserts as a function of the distance between the line source and the collimator aperture is given in Figure 2. The spatial resolution of the low-energy high-resolution (LEHR) collimator is plotted on the same graph for comparison. The sensitivity of the three pinhole collimator inserts and the LEHR collimator, as a function of distance between the disk

source and the collimator, are given in Figure 3. System sensitivity at the distance of 4.5 cm, used as the radius of rotation for animal studies, was 0.232 c/sec/kBq for the 3.3-mm aperture pinhole collimator, 0.086 c/sec/kBq for the 2.0-mm aperture pinhole collimator, and 0.023 c/sec/kBq for the 1.0-mm aperture pinhole collimator.

Figure 4A shows a transaxial image of the five-line source phantom used to measure the spatial resolution of the reconstructed SPECT images. Count profiles through transaxial slices of the reconstructed line sources were used to determine the spatial resolution in the transaxial plane (see Fig. 4B). The measured reconstructed transaxial in-plane resolution (FWHM) at 4.5-cm radius of rotation with the 2.0-mm collimator aperture averaged 2.8 mm.
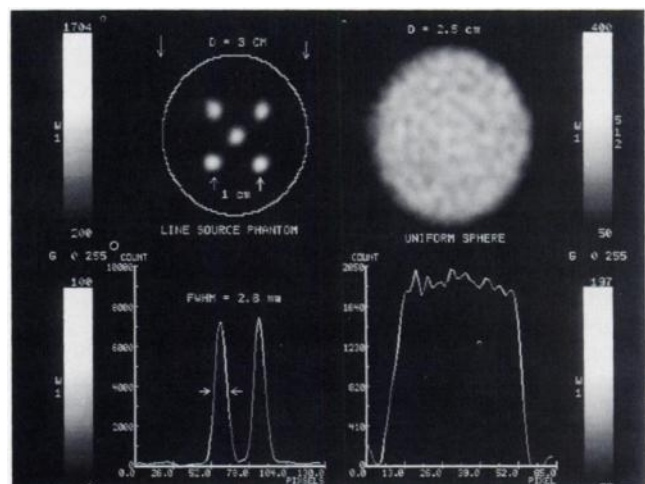

FIGURE 4. (A) Upper left: transaxial image of five-line source phantom used to measure spatial resolution. (B) Lower left: count profile of two-line sources from five-line source phantom. (C) Upper right: reconstructed transaxial slice through center of the 2.5-cm spherical phantom. (D) Lower right: count profile through transaxial slice of sphere filled with ^{99m}Tc shows typical variations in counts to be within ±5% of the mean.
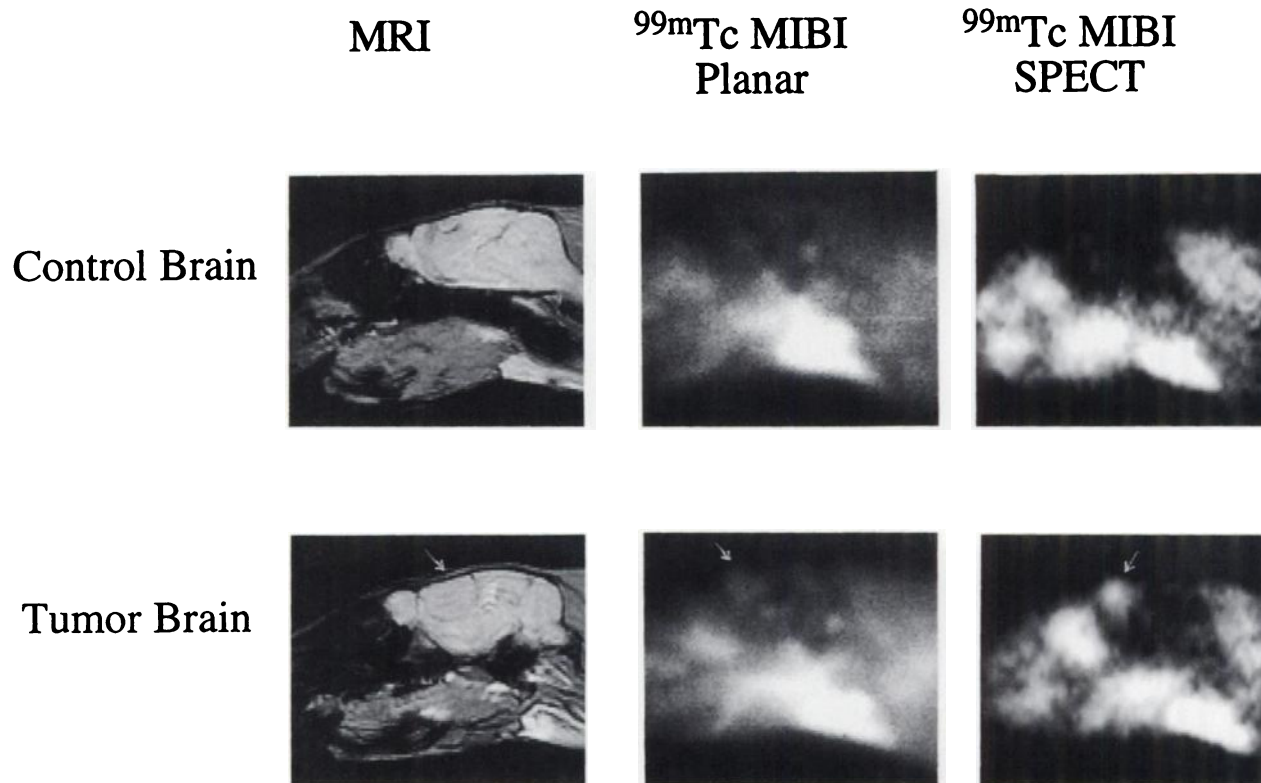
FIGURE 5. Upper row: (left) Sagittal MRI slice through the control rat's brain; (middle) left lateral planar image of ^{99m}Tc-MIBI localization in the control rat's brain shows uptake to occur in the regions of the pituitary gland and the choroid plexus; (right) sagittal SPECT slice in the same animal shows a minimal uptake of ^{99m}Tc-MIBI in the control brain. Lower row: (left) sagittal MRI slice through the brain reveals a gliosarcoma tumor encapsulated in the frontal region of the brain; (middle) left lateral planar image of ^{99m}Tc-MIBI uptake in the brain and tumor shows a region of increased activity at the site of the transplanted tumor and normal uptake in the area of the choroid plexus and pituitary gland; (right) sagittal SPECT slice in same animal shows focal uptake of ^{99m}Tc-MIBI only in the tumor. Arrows indicate tumor location.

Transaxial resolution did not vary significantly within the plane and between different planes. Figures 4C and D illustrate examples of a reconstructed transaxial image and a count profile across the center of the image from the 2.5-cm diameter ^{99m}Tc sphere used to test the correction for changes in geometric efficiency and uniformity. The test showed that counts in SPECT slices through the sphere were within ±5% of the mean counts across the FOV.

Brain Tumor

Figure 5 shows examples of sagittal magnetic resonance imaging (MRI) slices from a control rat's brain and from a tumor rat's brain with the corresponding planar left lateral scintillation camera images and the sagittal SPECT slice through the brain at the same level as the MRI slices. MRI shows the tumor to be located supratentorially in the frontal region. The well demarcated tumor in this example was approximately 6 mm in its major axis.

Planar posterior scintillation camera views and sagittal, coronal and transaxial pinhole SPECT images of the rat brain, in three rats studied with different radiopharmaceuticals and having similar tumors in the frontal region of the

brain, are shown in Figure 6. The posterior view is a 10-min planar image collected immediately following the SPECT acquisition. Each of the three sets of orthogonal slices shows four contiguous 2-pixel, 1.2-mm thick slices through the tumor. Comparison of ROIs over the tumor to uninvolved brain showed the tumor-to-brain uptake ratios (T/Br) to be: $T/Br_{(HMPAO)}$ = 0.5, $T/Br_{(MIBI)}$ = 8.6, $T/Br_{(^{201}Tl)}$ = 4.9, $T/Br_{(DTPA)}$ = 8.3 on the pinhole SPECT images, as compared to $T/Br_{(HMPAO)}$ = 0.8, $T/Br_{(MIBI)}$ = 1.9, $T/Br_{(^{201}Tl)}$ = 1.5, $T/Br_{(DTPA)}$ = 2.2 on the planar lateral pinhole scintillation camera images.

Figure 7 shows a beta-camera autoradiograph and a film autoradiograph of two, 50-μ thick coronal sections through the brain at the level of the tumor in a rat that received ^{99m}Tc-HMPAO. The T/Br ratio on the beta-camera autoradiograph was 0.5.

Myocardial Imaging

Another example of the level of spatial detail offered by pinhole SPECT is shown for ^{99m}Tc-MIBI localization in the myocardium of the rat. Figure 8 shows examples of the type of image quality and spatial resolution that can be achieved with pinhole SPECT following the administration
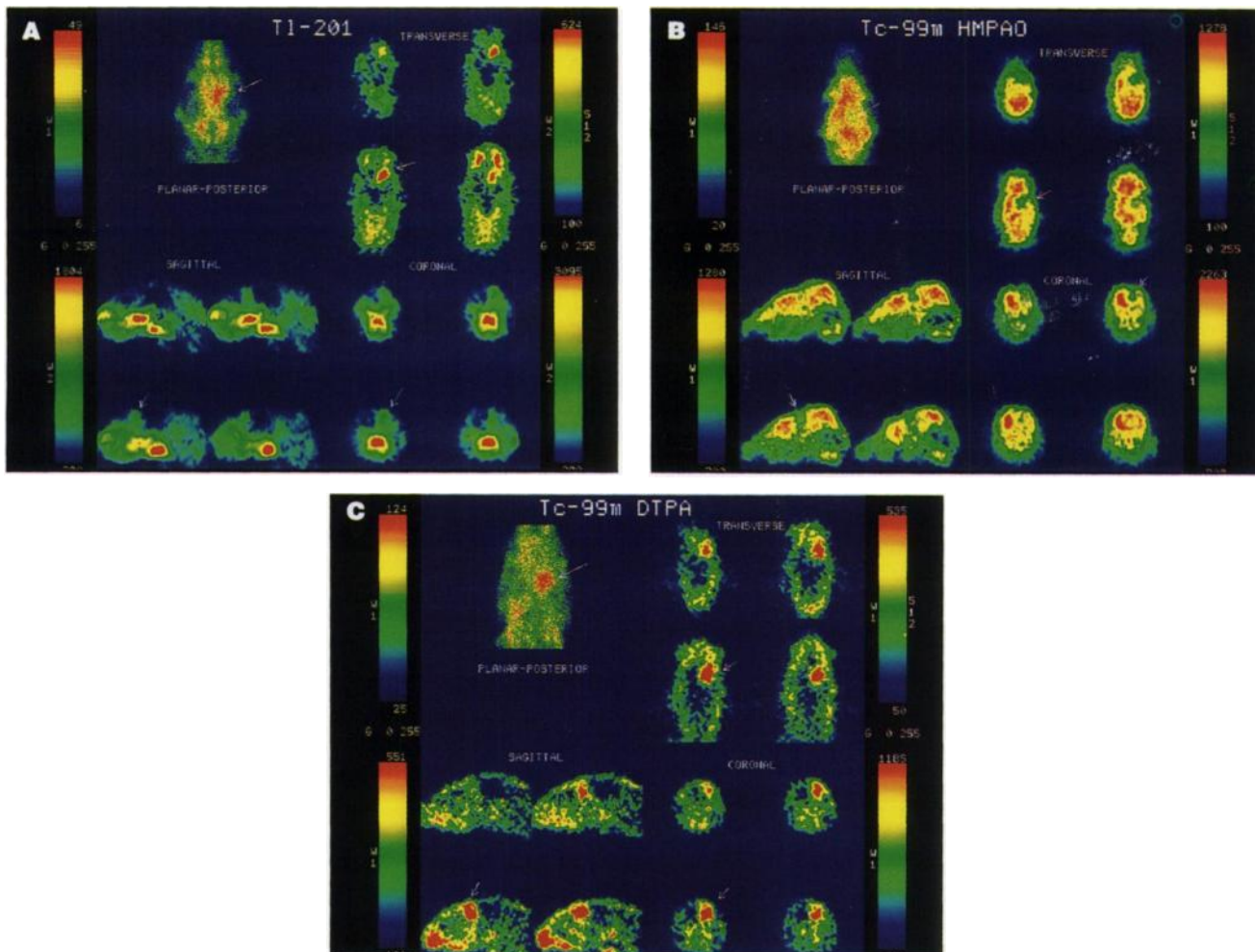
FIGURE 6. Comparative uptake properties of ^{201}TlCl, ^{99m}Tc-HMPAO and ^{99m}Tc-DTPA in brain and tumor in vivo by planar and SPECT imaging. Tumor is identified by an arrow in one slice on each set of orthogonal views. (A) Thallium-201-Cl posterior planar image shows increased activity in the left side of the brain; four contiguous 1.2-mm thick SPECT slices in the transverse, sagittal and coronal planes through the tumor reveal areas of intense, focally increased activity in the region of the tumor. (B) Technetium-99m-HMPAO posterior planar image shows a region with a small decrease in activity corresponding to the location of the tumor, whereas SPECT slices show a region of severely diminished activity in the same area. (C) Technetium-99m-DTPA posterior planar image shows a large region of abnormal uptake in the left hemisphere of the brain; SPECT slices clearly demonstrate an intense focus of abnormal uptake in the tumor with minimal activity contributed by surrounding structures.

of ^{99m}Tc-MIBI in the rat. The two series of SPECT slices are 2-pixel 1.2 mm thick long-axis and short-axis cuts through the myocardium.

DISCUSSION

Pinhole SPECT imaging provides high spatial resolution images of the localization properties of radiopharmaceuticals in small laboratory animals in vivo. Replacement of the commercially supplied pinhole inserts of 3.3, 4.8 and 6.9 mm in the pinhole collimator assembly with a pinhole aperture of 2.0 mm and implementing the modified cone-beam-filtered backprojection reconstruction algorithm (4), provided the basis for performing high-resolution SPECT with a conventional rotating gamma camera SPECT imaging system. Although a pinhole aperture insert made of tungsten would have been preferable to reduce the penetration of gamma photons through the edges of the aper-

ture, the lead insert was found adequate for the characteristic photon energies of ^{201}Tl and ^{99m}Tc. The calculated effective diameter of the 2-mm pinhole aperture made of lead is only 2.2% greater than an insert of the same dimensions fabricated of tungsten for the 140.5 keV photons of ^{99m}Tc (11). A tungsten collimator would need to be considered if higher energy photons were to be imaged. Restricting the radius of rotation for SPECT image acquisition to a distance of ≤4.5 cm for imaging the rat, yielded acceptable counting sensitivities and high spatial resolution images (Figs. 2 and 3). Of the three pinhole collimator apertures tested, the system sensitivity of 0.086 c/sec/kBq and a reconstructed spatial resolution of 2.8 mm with the 2.0-mm aperture at a radius of rotation of 4.5 cm provided the best combination of sensitivity and spatial resolution to obtain detailed images of the rat's brain and heart.

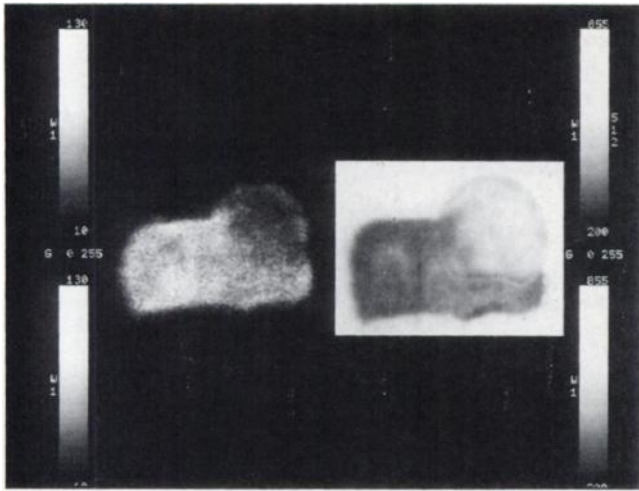Adequate counting levels were achieved for brain

FIGURE 7. Autoradiographs show the distribution properties of ^{99m}Tc HMPAO in 50-μ coronal sections through the brain and tumor of rat with transplanted gliosarcoma. The tumor shows greatly reduced perfusion. Left: beta-camera autoradiograph (*13*) provides direct quantitative assay of the distribution properties of the radiopharmaceutical. Right: film autoradiograph shows similar activity distribution for adjacent coronal section of the brain and tumor.

SPECT using acquisition times of ~45 min with administered activity doses of 37 MBq of ^{201}TlCl and 185 MBq of ^{99m}Tc-HMPAO, ^{99m}Tc-DTPA or ^{99m}Tc-MIBI. Very good quality SPECT images of the rat's heart were obtained using 185 MBq of ^{99m}Tc-MIBI with acquisition times of ~20 min. The spatial resolution of the pinhole collimator for an imaging distance of 4.5 cm from the collimator aperture is ~20% better than the intrinsic spatial resolution of the system for ^{99m}Tc and is significantly better than can be achieved with conventional parallel-hole, fanbeam or cone-beam collimation. At this imaging distance, the counting sensitivity is comparable to the LEHR collimator and the spatial resolution is better by almost a factor of 3 than that obtained with a LEHR collimator (Figs. 2 and 3).

Visual inspection of image quality with the 2.0-mm aperture pinhole SPECT images of the rat's brain and heart reveals excellent spatial detail of the distribution properties of radiopharmaceuticals tested. The 6-mm tumor seen in the MR image in Figure 5B is well demonstrated by focal uptake of ^{99m}Tc-MIBI on the sagittal slice through the middle of the tumor. Normal localization of ^{99m}Tc-MIBI in the choroid plexus and pituitary gland in the surrounding tissue is eliminated in the sagittal SPECT slice through the tumor. The improved visualization generally seen on pinhole SPECT images is demonstrated in Figure 6. Four contiguous 1.2-mm thick slices through the center of the tumor in the sagittal, coronal and transaxial planes of the brain of three rats are shown in comparison to the respective planar posterior scintillation camera views for three different radiopharmaceuticals. Here, the supratentorially located tumor is always better visualized on the SPECT slices than on the planar camera views. The tumor appears as a focus of abnormally elevated activity on the sagittal, coronal and transaxial slices with ^{201}Tl and ^{99m}Tc-DTPA,

and as a focus of abnormally decreased activity with ^{99m}Tc-HMPAO. With activity in overlying and underlying structures greatly decreased in the SPECT slice, excellent visualization of the localization properties is displayed.

The visualization of the distribution properties of radiopharmaceuticals in small structures seen on the pinhole SPECT images provides information by in vivo imaging which previously has been investigated primarily by autoradiography. An example of beta camera and conventional autoradiographs of brain tumor sections is shown in Figure 7. The level of detail of the activity distribution seen on ^{99m}Tc-HMPAO pinhole SPECT images (Fig. 6B), as compared to autoradiographs (Fig. 7) suggests that the improved spatial detail obtained by in vivo pinhole SPECT will be extremely useful for investigating new radiopharmaceuticals.

The combined sensitivity and spatial resolution offered by pinhole SPECT make high spatial resolution in vivo imaging feasible in small laboratory animals. Comparison of the activity ratios between tumor and control regions in the brain on SPECT and planar images validates the observations made by visual inspection. Activity ratios from ROIs placed over the tumor and in the brain outside of the tumor capsule show pinhole SPECT activity ratios to be significantly greater than observed on planar images. The combined high spatial resolution of the pinhole collimator and the major reduction in the overlying and underlying activity contribution in the reconstructed SPECT images account for these differences. The tumor-to-brain activity ratios on the pinhole SPECT images obtained by conventional ROI techniques are similar to those observed on the beta-camera autoradiograph of a 50-μ section through the tumor and brain and by well-cup counting of tissue specimens.

Although similar quantitation was not attempted on the myocardial images, the excellent spatial detail of the myocardial wall seen in the rat's beating heart is qualitatively

FIGURE 8. SPECT slices show myocardial uptake of ^{99m}Tc MIBI in the short-axis (upper two rows) and the long-axis (lower two rows) of the heart in the rat. Images were recorded without cardiac gating.

similar to that observed in the rat's brain (Fig. 8). The resolution properties of the pinhole collimator are sufficiently good to show regional localization properties without cardiac gating, and it is anticipated that these images could be significantly improved if image gating was employed.

The improved spatial resolution properties offered by pinhole SPECT presents major opportunities to perform detailed imaging studies of radiopharmaceuticals in vivo. The approach provides the means to perform serial and repeat imaging studies in the same living animal at multiple times to investigate tumor growth, tissue pathology, effects of therapy, intervention and activation. Application of pinhole SPECT imaging should lead to a reduction in the number of animals needed to perform radiopharmaceutical distribution studies and could provide an accurate mapping of regional localization with and without intervention in vivo. The pinhole SPECT procedure should be suitable for performing high-resolution imaging of the hands and wrist in clinical studies; suitable optimization of the size of the pinhole aperture with a small acquisition distance could extend applications to imaging the thyroid gland and the cervical spine.

ACKNOWLEDGMENTS

REFERENCES

1. Serafini AN. From monoclonal antibodies to peptides and molecular recognition units: an overview. J Nucl Med 1993;34:3(suppl.):533–536.
2. Weber DA, Kassis AI, eds. Radiolabeled antibody tumor dosimetry. Med Phys 1993;20:497–610.
3. Stadalnik RC, Kudo M, Eckelman WC, Vera DR. In vivo functional imaging using receptor-binding radiopharmaceuticals. Clin Radiol 1993;28:64–70.
4. Erlandsson K, Ivanovic M, Strand S-E, Sjögren K, Weber DA. High resolution pinhole SPECT for small animal imaging [Abstract]. J Nucl Med 1993;34:9P.
5. Erlandsson K, Ivanovic M, Strand S-E, Weber DA. Pinhole SPECT: a high resolution technique for tumor imaging [Abstract]. Antibody Immunoconj and Radiophar 1992;5:356.
6. Feldcamp LA, Davis LC, Kress JW. Practical cone-beam algorithm. J Opt Soc Am 1984;1:612–619.
7. Gullberg GT, Zeng GL, Datz FL, Christian PE, Tung C-H, Morgon HT. Review of the convergent beam tomography in single photon emission computed tomography. Phys Med Biol 1991;37:507–534.
8. Palmer J, Wollmer P. Pinhole emission computed tomography: method and experimental evaluation. Phys Med Biol 1990;35:339–350.
9. Rogers WL, Slosar J, Hua L, Chiao P, Zhang Y, Clinthorne NH. A high resolution slit aperture for imaging small animals with SPECT [Abstract]. J Nucl Med 1993;34:9P.
10. Jaszczak RJ, Li J, Wang H, Zalutsky MR, Coleman RE. Pinhole collimation for ultra-high resolution small-field-of-view SPECT studies [Abstract]. J Nucl Med 1993;34:9P.
11. Anger HO. Radioisotope cameras. In: Hine GJ, ed. Instrumentation in nuclear medicine. New York: Academic Press; 1967:485–552.
12. Joel DD, Fairchild RG, Laissue JA, Saraf SK, Kalef-Ezra JA, Slatkin DN. Boron neutron capture therapy of intracerebral rat gliosarcomas. Proc Natl Acad Sci 1990;87:9808–9812.
13. Ljunggren K, Strand S-E. Beta camera for static and dynamic imaging of charged-particle emitting radionuclides in biological samples. J Nucl Med 1990;31:2058–2063.